

# The centre-to-limb variations of solar Fraunhofer lines imprinted upon lunar eclipse spectra

## Implications for exoplanet transit observations

F. Yan<sup>1,2,3</sup>, R. A. E. Fosbury<sup>3</sup>, M. G. Petr-Gotzens<sup>3</sup>, G. Zhao<sup>1</sup>, and E. Pallé<sup>4,5</sup>

<sup>1</sup> Key Laboratory of Optical Astronomy, National Astronomical Observatories, Chinese Academy of Sciences, 20A Datun Road, Chaoyang District, 100012 Beijing, China  
e-mail: feiy@nao.cas.cn, gzhao@nao.cas.cn

<sup>2</sup> University of Chinese Academy of Sciences, 19A Yuquan Road, Shijingshan District, 100049 Beijing, China

<sup>3</sup> European Southern Observatory, Karl-Schwarzschild-Str. 2, 85748 Garching bei München, Germany

<sup>4</sup> Instituto de Astrofísica de Canarias, C/ vía Láctea, s/n, 38205 La Laguna, Tenerife, Spain

<sup>5</sup> Dpto. de Astrofísica, Universidad de La Laguna, 38206 La Laguna, Tenerife, Spain

Received —; accepted —

### ABSTRACT

The atmospheres of exoplanets are commonly studied by observing the transit of the planet passing in front of its parent star. The obscuration of part of the stellar disk during a transit will reveal aspects of its surface structure resulting from general centre-to-limb variations (CLVs). These become apparent when forming the ratio between the stellar light in and out of transit. These phenomena can be seen particularly clearly during the progress of a penumbral lunar eclipse, where the Earth transits the solar disk and masks different regions of the solar disk as the eclipse progresses. When inferring the properties of the planetary atmosphere, it is essential that this effect originating at the star is properly accounted for. Using the data observed from the 2014-April-15 lunar eclipse with the ESPaDOnS spectrograph mounted on the Canada France Hawaii Telescope (CFHT), we have obtained for the first time a time sequence of the penumbral spectra. These penumbral spectra enable us to study the centre-to-limb variations of solar Fraunhofer lines when the Earth is transiting Sun. The Na I and Ca II absorption features reported from previous lunar eclipse observations are demonstrated to be CLV features, which dominate the corresponding line profiles and mask possible planetary signal. Detecting atmospheric species in exoplanets via transit spectroscopy must account for the CLV effect.

**Key words.** planets and satellites: atmospheres – eclipse – Earth

## 1. Introduction

With the discovery of almost 2000 exoplanets in the last two decades, the characterisation of their atmospheres has become a new and rapidly-evolving field. Different atomic, ionic, and molecular species have already been detected in exoplanet atmospheres. Using Hubble Space Telescope data, Charbonneau et al. (2002) detected sodium in the atmosphere of HD 209458b for the first time by comparing the Na I doublet absorption lines in and out of transit. Snellen et al. (2008) then confirmed the Na I absorption in HD 209458b using ground-based telescope data. Sodium has also been detected in several other giant exoplanets such as HD 189733b (Redfield et al. 2008) and WASP-17b (Wood et al. 2011). Potassium was detected in HD 80606b (Colón et al. 2012) and XO-2b (Sing et al. 2011), while Fossati et al. (2010) reported the detection of Mg II in WASP-12b. All of these used transmission spectroscopy during transits. Molecular features have also been detected in exoplanet atmospheres, such as H<sub>2</sub>O (Grillmair et al. 2008), CO (Brogi et al. 2012), CO<sub>2</sub> (Swain et al. 2009), and CH<sub>4</sub> (Swain et al. 2008).

In recent years, nearly 100 Earth-sized or smaller exoplanets have been discovered, one of them being in the habitable zone of its host star (Quintana et al. 2014). Although character-

ising the atmospheres of these terrestrial exoplanets is not within the reach of current instrumentation, the detection of some their atomic and molecular components is very likely to become possible with the next generation of large ground- and space-based telescopes (Hedelt et al. 2013). The Earth itself can be used as a benchmark for the future detection of Earth-like exoplanets, for example, using lunar eclipses to obtain the tangential long-path transmission spectrum of the Earth's atmosphere.

Several lunar eclipse observations have been made with the aim of obtaining the transmission spectrum of the Earth's atmosphere. Some of these have reported the anomalous behaviour of certain atomic absorption features. Pallé et al. (2009, hereafter P09) observed the lunar eclipse of 16 August 2008, and obtained transmission spectra from the umbral lunar eclipse. In P09's spectra, the Ca II absorption features are detected and weak Na I absorptions also appear. Vidal-Madjar et al. (2010, hereafter V10) observed the same lunar eclipse as P09, but they retrieved the transmission spectrum from the penumbral rather than the umbral eclipse. In V10, the authors detected relatively strong Na I D lines absorption but no Ca II absorption. Arnold et al. (2014, hereafter A14) observed the penumbral lunar eclipse in December 2010 and their results are similar to those of V10, i.e. Na I absorption is detected while Ca II is not. Yan et al. (2014) observed the lunar eclipse of December 2011 and neither the Na I

nor the Ca II absorption features are detected in the transmission spectrum obtained from the umbral eclipse.

The interpretation of these discrepancies is not straightforward since the Earth’s transmission spectra from these observations are retrieved using different methods. Although there are Na I, Ca I, and Ca II layers in the Earth’s ionosphere, according to our research, the Na I or Ca II absorption features in the observed Earth’s transmission spectra are probably due to the centre-to-limb variation (CLV) of the solar lines rather than the absorptions in the Earth’s atmosphere.

The strong solar Fraunhofer lines have prominent variations in both line intensity and profile from centre to limb across the solar disk. Athay et al. (1972) used the Fe I line’s CLV spectrum to generally interpret the CLV effect. For most strong solar Fraunhofer lines, the normalised spectral line from the centre of the disk is deeper than that from the limb. The observed CLV features are used to understand detailed solar physics and to guide the modelling work. For example, Allende Prieto et al. (2004) observed the CLV of solar lines and used this to test non-Local Thermodynamic Equilibrium line formation calculations and Koesterke et al. (2008) used the CLV data to test 3D solar hydrodynamic simulations.

Since a lunar eclipse shares similarities with an exoplanet transit, this CLV effect can also be present in transit spectra. The corresponding features will be considerably weaker since the planet only blocks a small fraction of the stellar surface during transit. However, the CLV effect can still have an influence on the interpretation of atomic line detections in exoplanet atmospheres and should be properly treated.

For the detection of sodium in HD 209458b, Charbonneau et al. (2002) considered the CLV in the Na I D lines and concluded that the contribution was small for their observation. Redfield et al. (2008) modelled the CLV effect on the Na I D lines in HD 189733b (the CLV is referred to as differential limb darkening in their paper), and the model shows that this contribution is much smaller than the observed Na I absorption. However, for stellar lines that have significant CLV effects or if the observation is performed at high spectral resolution, this effect could become important.

We observed the lunar eclipse in April 2014 and obtained a set of spectra at different stages of the eclipse. The changes in the solar line profiles caused by the CLV can clearly be seen in our data. In Section 2, we use our lunar eclipse data to demonstrate this effect and compare it with the solar spectral Atlas. In Section 3, the Na I and Ca II features observed in previous lunar eclipse observations are compared with the spectral features caused by CLV. In Section 4, we further discuss the CLV effect on exoplanet transit spectroscopy. The telluric sodium absorption and the Raman scattering in lunar eclipse spectra are also discussed in Section 4.

## 2. The effect of CLV on lunar eclipse observations

A penumbral lunar eclipse happens when the Moon enters the Earth’s penumbral shadow. An observer on the Moon in the penumbra would see the Earth blocking different parts of the solar disk (as shown in Fig. 1). Thus the penumbral spectrum comprises the integrated spectrum of the Sun, which is partly eclipsed by the Earth. When observing different locations on the Moon in the Earth’s penumbra, the observed spectra are integrated from different parts of the solar disk. Since the solar lines vary in profile from the centre to limb, the line profiles in the penumbral spectra vary as the eclipse proceeds. For the spectrum observed from the un-eclipsed Moon (which is called the bright

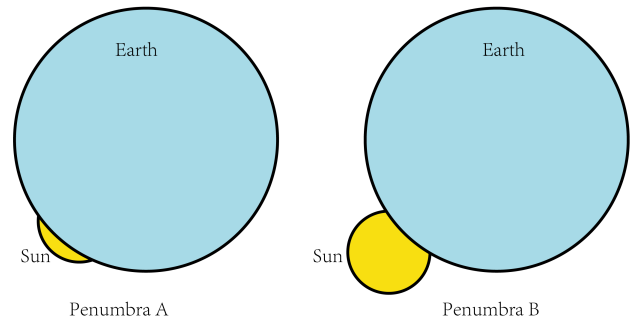


**Fig. 1.** A schematic of a penumbral eclipse as seen from the Moon. Here Penumbra A and Penumbra B represent the views from two different penumbral locations (indicated in Fig. 2).

Moon), it is the integration of the entire solar disk. The umbral spectrum results from the integrated light of the solar disk that is refracted by the Earth’s atmosphere into the umbral shadow (García Muñoz et al. 2012). The line shape in the umbral spectrum varies, depending on which part of the solar disk has been refracted. However, the line shape difference between the umbral spectrum and the bright Moon spectrum is relatively small, and the penumbral spectrum exhibits significant differences (see Fig. 3 for details).

### 2.1. The April 2014 lunar eclipse observations

We used the fiber-fed ESPaDOnS spectrograph mounted on the Canada France Hawaii Telescope (CFHT) for our observations. The spectrograph covers a wavelength range of 370–1050 nm in a single exposure. The ‘object only’ mode was used to achieve high spectral resolving power (average resolution:  $\lambda/\Delta\lambda \sim 81,000$ ). The observation began when the Moon was in the Earth’s umbra and lasted until the Moon was fully out of the Earth’s shadow. We used non-sidereal tracking to locate the fiber at the Eudoxus crater during the entire observation. The Eudoxus crater is chosen because it enables us to access different phases of the umbral eclipse as its trace is close to the umbral center. Fig. 2 shows the trace of Eudoxus with respect to the Earth’s shadow. We obtained a sequence of spectra from the umbra, penumbra, and bright Moon, and we performed the standard data reduction procedure using the CFHT Upena pipeline<sup>1</sup>.

The penumbral spectral sequence consists of about 60 spectra from different penumbral locations, enabling us to study the line shape change. We label the location close to the umbra as Penumbra A and the location close to the bright Moon as Penumbra B (Fig. 1 and Fig. 2). Fig. 3 shows the changes of the H $\alpha$  line profile. The spectra in this figure are the ratios of the penumbral spectra to a bright Moon spectrum. The bottom of this figure shows the ratio of a typical umbral to the bright Moon spectrum for comparison.

At the beginning of our penumbral eclipse observation (corresponding to Penumbra A), the line shape is generally shallower than that in the bright Moon spectrum, which results in the ‘emission’ feature in Fig. 3. As the eclipse proceeds, the H $\alpha$  line becomes deeper. When the observed location is close to Penumbra B, the H $\alpha$  line becomes the deepest, even deeper than in the bright Moon spectrum. As this change of the H $\alpha$  line

<sup>1</sup> <http://www.cfht.hawaii.edu/Instruments/Upena/>

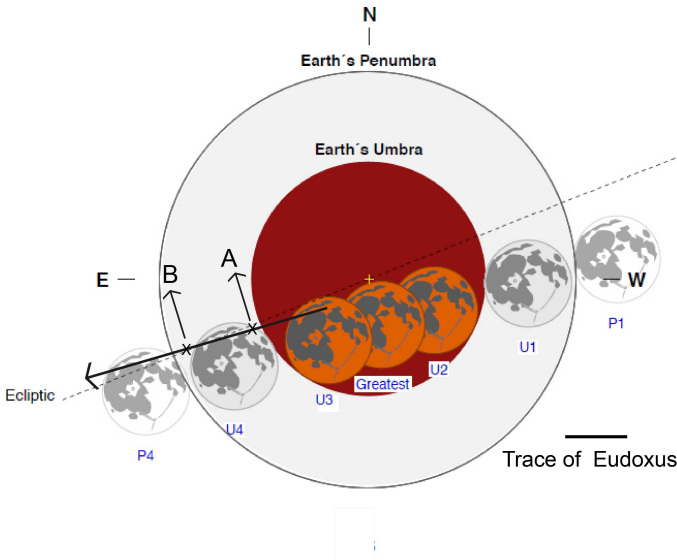


**Fig. 2.** The trajectory of the observed Eudoxus crater for the 15 April 2014 lunar eclipse. The arrow on the trajectory indicates the moving direction of the crater. Here we choose two points on the trajectory (A and B) to indicate different eclipsing stages. Point A and B correspond to the Penumbra A and Penumbra B views sketched in Fig. 1. The figure is reproduced from the NASA eclipse website (<http://eclipse.gsfc.nasa.gov/lunar.html>).

shape is correlated with the eclipse geometry, we conclude that it results from the CLV effect.

Since previous studies of lunar eclipse observations use the penumbral spectrum obtained at a position close to the umbra (i.e. Penumbra A), we will only discuss this type of penumbral spectrum below.

## 2.2. CLV features in the spectrum

Fig. 4a displays the ratio of an observed penumbral to a bright Moon spectrum. Here the penumbral spectrum was taken when the observed location was close to the umbra, which means the penumbral spectrum is mainly from the limb part of the solar disk (corresponding to Penumbra A in Fig. 1). In contrast, the bright Moon spectrum is from the whole solar disk and so it is the mix of limb and centre solar spectra. This spectral ratio can therefore be qualitatively regarded as the limb to centre spectrum plus a constant. It can be seen in Fig. 4a that the solar line features clearly show up especially towards the blue part of the spectrum. Strong absorption lines such as the Ca II T (Ca II near-infrared triplet), Ca II H & K, H $\alpha$ , H $\beta$ , and the Mg I b lines appear prominently while the Na I D lines features are relatively weak.

To better demonstrate the CLV effect in a lunar eclipse, the solar spectrum from the Kitt Peak Solar Atlas (Brault & Testerman 1972; Kurucz 2005) is used as a comparison. The Atlas comprises two sets of spectra: one observed at the centre of the solar disk with  $\mu = 1.0$  (where  $\mu = \cos(\theta)$ ,  $\theta$  is the angle between the normal to the solar surface and the line of sight) and the other at a limb position with  $\mu = 0.2$ . All the spectra were taken when the Sun was quiet. The ratio of the centre to limb Solar Atlas is shown in Fig. 4b and one can see that the overall features are very similar to those in Fig. 4a.

These general features show that the strong Fraunhofer lines are deeper in the centre than in the limb spectrum, which means the mean limb-darkening within the spectral line is less pro-

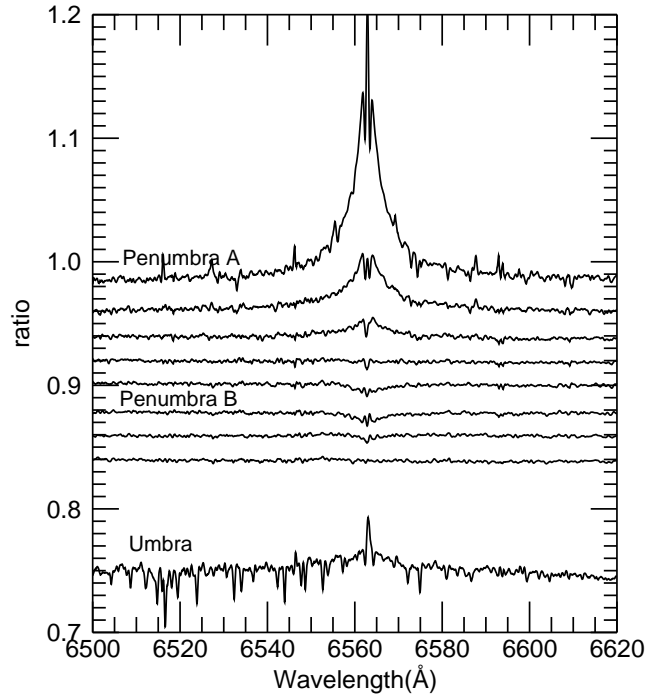


**Fig. 3.** The change of H $\alpha$  line shape in different penumbra spectra. The spectra are the ratios of the normalised penumbral to bright Moon spectra. The ratios are shifted sequentially by 0.02 for clarity. Eight penumbral spectra which were taken every ten minutes are chosen to represent different penumbral locations. The upper spectrum corresponds to the penumbral position close to the umbra (Penumbra A in Fig. 2), while the lower spectrum corresponds to the position close to the bright Moon (Penumbra B in Fig. 2). The normalised ratio of the umbral to the bright Moon spectrum is also shown at the bottom of the figure for comparison. This umbral spectrum is the sum of seven individual exposures that were taken at positions close to the edge of the umbra (i. e. close to Penumbra A). The total observed time for this umbral spectrum is about 20 minutes. The umbral spectrum has a relatively low signal-to-noise ratio and strong telluric absorption lines. The radial velocity differences between these spectra have been corrected.

nounced than in the adjacent continuum (Athay 1972). The continuum limb darkening is more prominent at blue/UV wavelengths because of the amplification of the temperature induced intensity variation in the Wien side (short wavelength region) of the blackbody curve. This also makes the mean CLV features become more significant for the lines located at the blue/UV wavelengths.

In addition to the general CLV features described above, the detailed profile has a complicated structure, which differs from line to line. For example, the line core becomes broader in the limb spectrum than in the centre spectrum, which makes the line core CLV feature differ from that of the line wing. This can be seen for example in the Ca II T and Na I D lines shown in Fig. 5 and 6. The line core CLV is due to the Doppler broadening, which is stronger in the limb than in the centre spectrum. This differential Doppler broadening may be interpreted either as an increased Doppler velocity with height or as an anisotropy in the Doppler velocity field where the horizontal velocity exceeds the vertical velocity (Athay 1972). Other solar phenomena such as the convective motion of the granules (Dravins 1982) also contribute to the detailed CLV features, but these are beyond the scope of this paper.

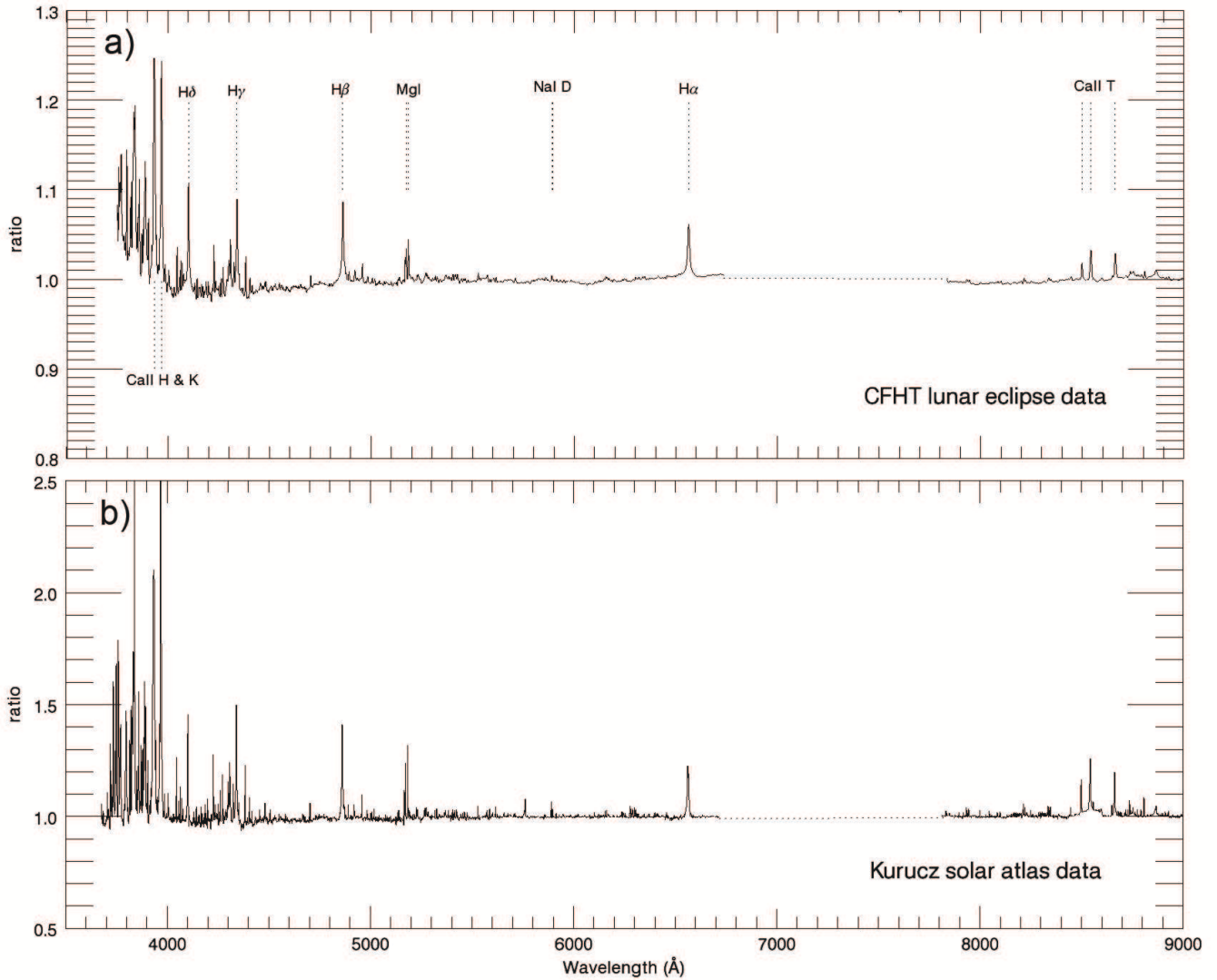


**Fig. 4.** (a) The ratio of a penumbral spectrum to a bright Moon spectrum observed on April 15 2014 by CFHT. The solar lines features remain in the ratio spectrum. The data is binned to a low resolution and the RV difference between the two spectra has been corrected. The dashed line region is where the telluric  $\text{H}_2\text{O}$  and  $\text{O}_2$  lines are prominent. They are not shown here as we concentrate on the solar spectral feature. (b) The ratio of the limb solar spectrum to the centre solar spectrum. The data are from the Kitt Peak Solar Atlas and binned to a low resolution.

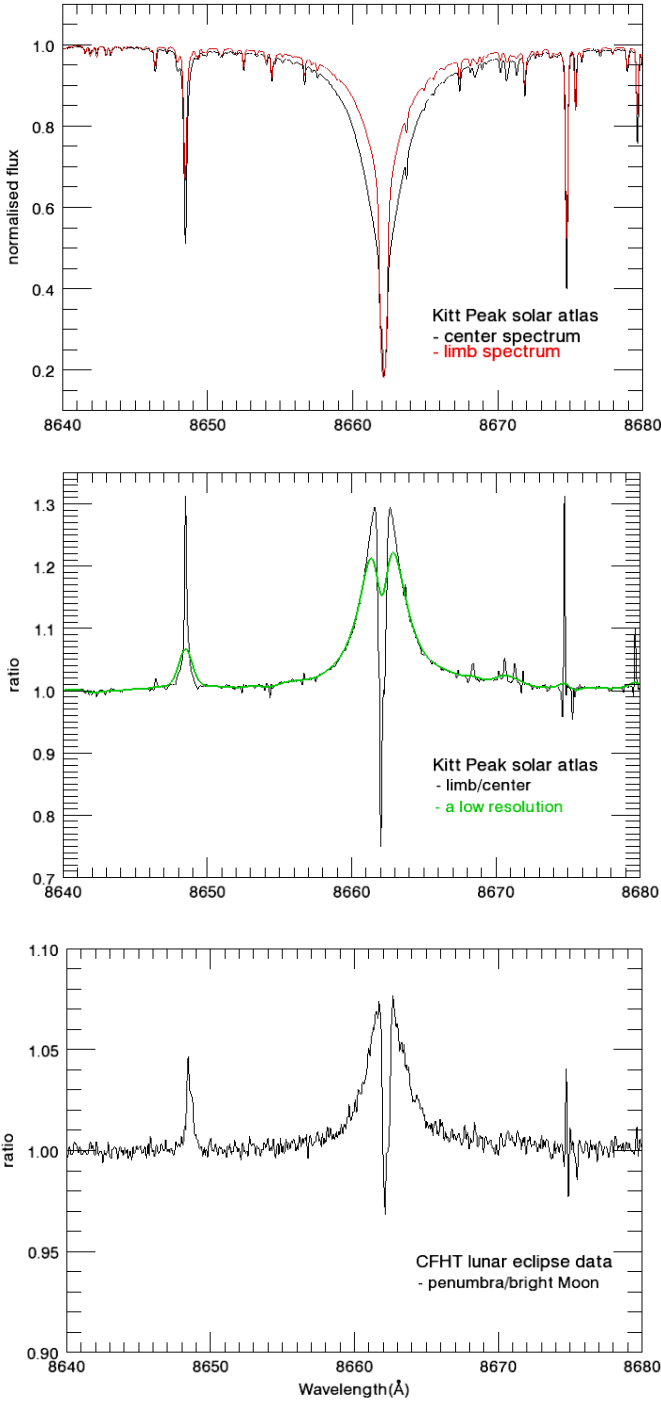
### 3. $\text{Ca II}$ and $\text{Na I}$ features in lunar eclipse observations

Since ionised calcium and neutral sodium are present in the Earth’s ionosphere and previous studies of lunar eclipse observations claimed the detection of their absorption lines, it is important to understand how the solar CLV affects their detections in the Earth’s transmission spectrum. For the CLV of the  $\text{Ca II}$  Fraunhofer lines (e.g. the  $\text{Ca II T}$  and  $\text{Ca II H\&K}$ ), we choose the  $\text{Ca II}$  8662 Å line as a demonstration. Fig. 5 shows the 8662 Å line from both the Kitt Peak Solar Atlas and the CFHT lunar eclipse data. The ratio of the solar limb to centre spectrum (middle panel in Fig. 5) and the ratio of penumbra to bright Moon spectrum (bottom panel) are quite similar. Fig. 6 shows the  $\text{Na I D}_2$  line at 5889 Å. The CLV feature of the  $\text{Na I D}_2$  line is similar to, but much weaker than, the  $\text{Ca II T}$  lines. In the middle panel of this figure, the one Å resolution spectrum (shown as the green line) smears the feature, indicating how the instrumental resolution can affect the observed strength of the CLV feature.

#### 3.1. $\text{Ca II}$ and $\text{Na I}$ features in previous low spectral resolution observation

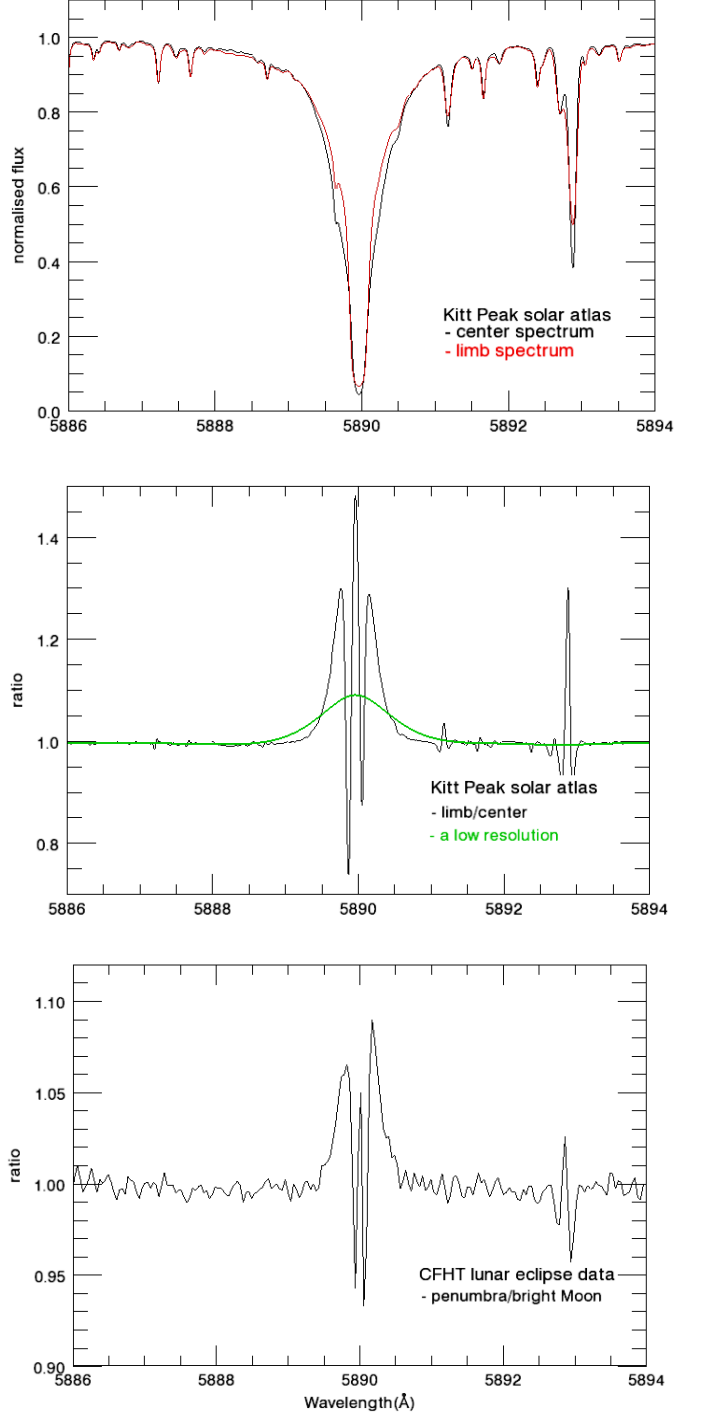
Pallé et al. (2009) observed the 16 August 2008 lunar eclipse at a relatively low resolution (6.8 Å in the optical wavelength range). They regarded the penumbral spectrum as the reference spectrum and obtained the Earth’s transmission spectrum by using the ratio of the umbral to the penumbral spectrum to cancel out the solar spectral features. However, because of the CLV, the solar absorption line profiles are different in the umbral and penumbral spectra. The solar line shapes in the umbral spectrum are similar to the bright Moon spectrum while the line shapes in the penumbral spectrum have a significant CLV effect. Thus the  $\text{Ca II T}$  and  $\text{Ca II H\&K}$  lines, as well as the weak  $\text{Na I D}$  lines absorption features in P09’s transmission spectrum, are most likely to be the result of the CLV effect.

Figure 7 shows the detailed features at the positions of the  $\text{Ca II T}$  lines. Here the ratio of the centre to limb spectrum from the Kitt Peak Solar Atlas (Fig. 7a) is used to mimic the umbral to penumbral spectral ratio. Our CFHT data are also shown for



**Fig. 5.** The detailed line shape of Ca II 8662 Å line. Top panel: the limb and centre spectra from the Kitt Peak Solar Atlas. Middle panel: the ratio of the limb to centre Kitt Peak spectrum. The green line is same data convolved to 1 Å resolution. Bottom panel: the ratio of the penumbra to bright Moon spectrum from CFHT lunar eclipse data (the same data set as shown in Fig 4a).

comparison. Fig. 7b is the ratio of the bright Moon spectrum to the penumbral spectrum from the CFHT observation and it shows a behaviour very similar to that constructed from the Solar Atlas. Fig. 7d shows the same data as in Fig. 7b but convolved to the resolution of the P09 data. It is clear that the CLV feature in the CFHT data is similar to the spectrum in P09 (Fig. 7c).



**Fig. 6.** The same as Fig. 5 but for Na I D<sub>2</sub> line at 5890 Å .

The Na I D line features are relatively weak in P09. This is interpreted as CLV features of the Na I doublet being weaker than other strong Fraunhofer lines and consequently not strongly apparent at low resolution.

### 3.2. Na I features in previous high spectral resolution observations

Vidal-Madjar et al. (2010) observed the 16 August 2008 lunar eclipse with high-resolution spectroscopy and they obtained the transmission spectrum by using the ratio of the penumbral to the

bright Moon spectrum. In their resulting transmission spectrum, the Na I D features are not well cancelled out and the zero level shift (an offset of the spectral counts) is applied to correct the broad features at Na I D positions (Fig. 10 in V10). This correction results in a deeper 'absorption' feature at the line centre, which the authors interpret to be the atomic sodium absorption of the Earth's atmosphere. However, we conclude that this is the CLV feature of the Na I D lines and the feature at the line core originates from the differential Doppler broadening between the centre and limb solar spectra as discussed in Section 2.2.

Arnold et al. (2014) observed the 21 December 2010 lunar eclipse with two high-resolution ESO spectrographs: HARPS and UVES. They applied a similar method as V10 and obtained the high-resolution transmission spectrum from the penumbral spectrum. In the resulting transmission spectrum from HARPS, the Na I D features occur (Fig. 9 in A14) and the authors use a Raman scattering model to correct the broad signature of the line wing (the Raman scattering will be discussed in the next section). This correction again results in a deeper 'absorption' feature at the line core, which is similar to the result in V10. They also applied a wavelength-dependent limb darkening to correct the penumbral spectrum. The limb darkening they used is a low-resolution model (several nanometres), thus it only corrects the limb darkening of the continuum while the CLV of the Na I D line remains in the ratio of the penumbral to the bright Moon spectrum.

We reanalysed the HARPS data from the 21 December 2010 lunar eclipse using the ratio of the bright Moon to penumbral Moon spectrum to simulate the effective altitude calculation method (Equation 2 in A14). Fig. 8 shows the result of our simulation. The top panel is the original ratio of the bright Moon to the penumbral Moon spectrum. This is similar to the bottom figure of Fig. 16 in A14. The middle panel is the ratio spectrum after the radial velocity (RV) correction. The RV difference between the bright Moon and the penumbral Moon is due to the motion between the Earth, Moon, and Sun, as well as the Rossiter-McLaughlin effect (Yan et al. in preparation). We correct this RV difference to perfectly align the solar spectral lines. After the RV correction, the CLV feature of the Na I D lines appears clearly, and is similar to Fig. 9 in A14. The bottom panel in Fig. 8 is the ratio of the centre to limb spectrum from the Kitt Peak Solar Atlas and it corresponds closely to the feature from the lunar eclipse observation.

In fact, the Na I D feature in V10 is basically the same as that in A14 except at a lower resolution. As the spectrum of P09 is in a much lower resolution, the Na I D feature in P09 is only marginally observed. By comparing the Na I D feature in the three papers, we can see that the appearance of the CLV feature is affected by the data analysis method, spectral resolution, and the radial velocity correction.

## 4. Discussion

### 4.1. The forward-scattered sunlight and the Ring effect

The forward-scattered sunlight from the Earth's terminator atmosphere also contributes to the irradiance of the eclipsed Moon (Link 1972; Vollmer & Gedzelman 2008). In the forward-scattered sunlight, there is a Raman scattering component that transfers continuum photons into a solar absorption line to make the scattered line shallower. This filling-in of Fraunhofer lines is called the Ring effect (Grainger & Ring 1962) and can change the solar line shape in a lunar eclipse spectrum (Yan et al. 2014). This Ring effect was employed by A14 to correct the line shape

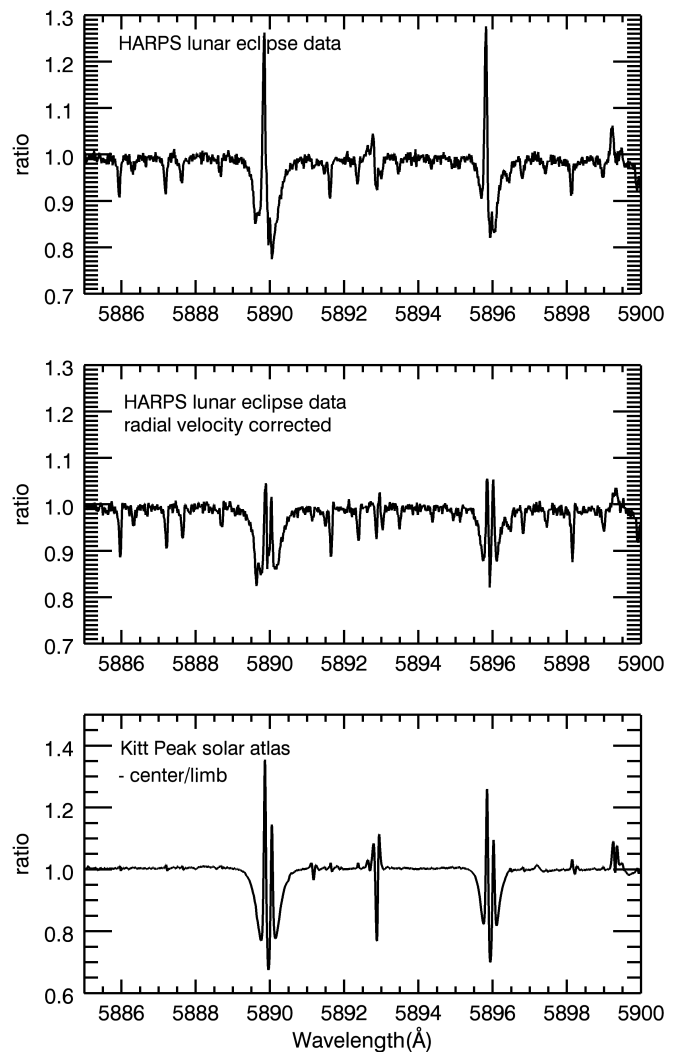


**Fig. 8.** The CLV features in the Na I D lines. Top panel: ratio of the bright Moon to penumbral spectrum from the HARPS observation in December 2010. Middle panel: same as top, except with the radial velocity corrections applied. Bottom panel: the centre to limb spectrum from the Kitt Peak Solar Atlas.

of Na I D doublet. Below we quantitatively discuss the Ring effect contribution in both the umbral and penumbral spectra.

García Muñoz & Pallé (2011) modelled the forward-scattered sunlight spectrum during a lunar eclipse. Their result shows that, at wavelength around Na I D doublet, the typical amount of the forward-scattered sunlight received at the lunar surface is  $2 \times 10^{-7}$  of the flux from the unobstructed Sun (i. e. the bright Moon). The amount here is for the atmospheric model containing molecular and aerosol scattering and O<sub>3</sub> absorption, i. e. model dIII in García Muñoz & Pallé (2011). In order to estimate the contribution of the scattered light, we use our CFHT observation to generate an eclipse light curve. Fig. 9 shows the observed fluxes, which are normalised to a bright Moon spectrum taken at the meridian. The flux of the forward-scattered sunlight can be regarded as constant since it is a diffuse component and the scattering angle changes little during the eclipse. It is clear that the scattered light proportion is larger for an eclipse spectrum taken at a position close to the umbral center where the irradiance of the lunar surface is small. For the umbral spectrum, the scattered light proportion

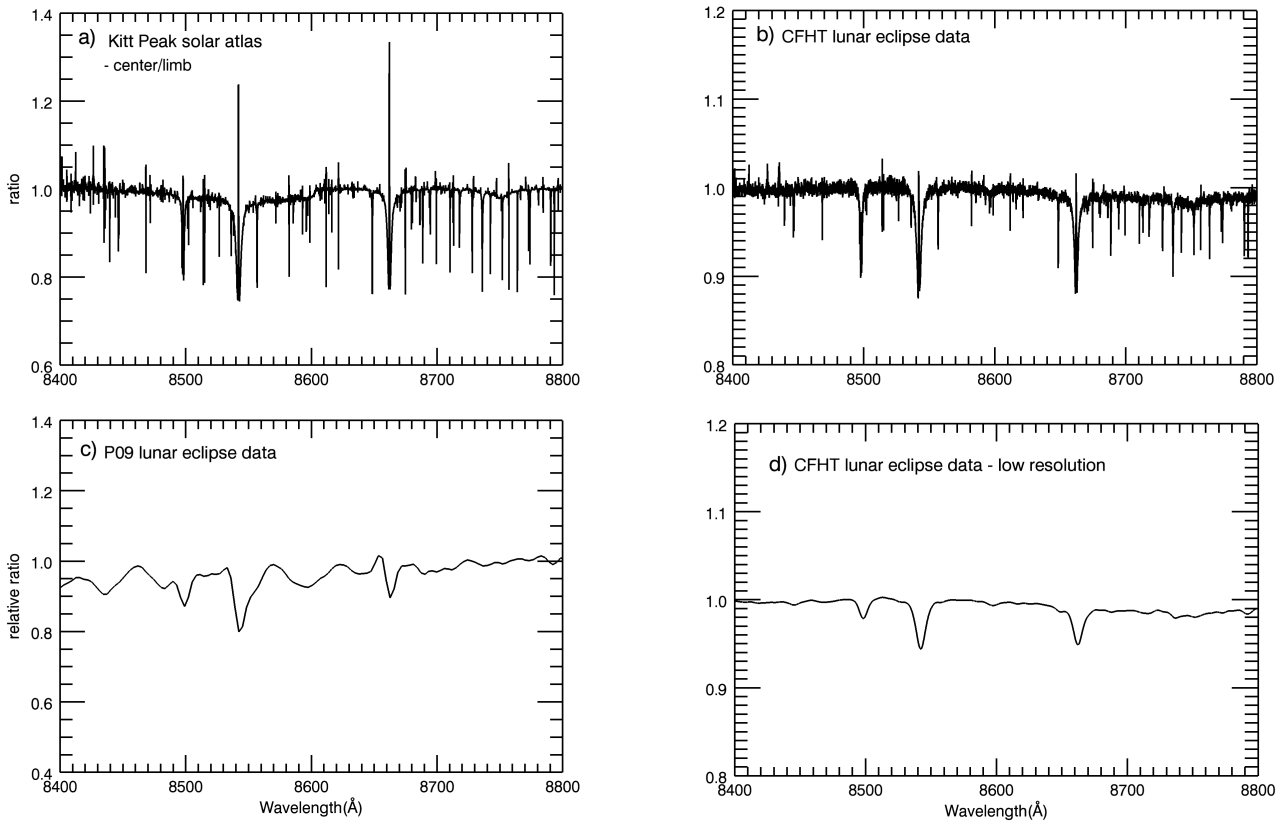


**Fig. 7.** The CLV features in the Ca II T lines. (a) Top left: ratio of the centre to limb spectrum from the Kitt Peak Solar Atlas. (b) Top right: ratio of the bright Moon spectrum to the penumbral spectrum from our CFHT data. (c) Bottom left: the Ca II T feature in P09’s transmission spectrum. (d) Bottom right: the same as (b) except convolved to the resolution of P09 data.

can range from 0.01 to  $10^{-4}$ . For the penumbral spectrum, the proportion is determined mainly by the portion of the unobstructed solar disk and ranges from  $10^{-4}$  to  $2 \times 10^{-7}$ . For example, the amount of scattered light is on the order of  $10^{-5}$  for Penumbra A (Fig. 1) where about 1/6 of the solar disk can be seen.

In the forward-scattered sunlight, the rotational Raman scattering transfers a few percent of the continuum photons into the Fraunhofer lines at UV to optical wavelengths (Noxon et al. 1979; Langford et al. 2007). For an eclipse spectrum taken close to the umbral center, this Raman scattering transfers roughly  $10^{-4}$  of the continuum into the lines after taking the forward-scattering sunlight proportion in the total irradiance into account. The spectra taken at a position away from the umbral center will have a lower filling-in effect. Here the estimation is for wavelengths around 600 nm, however, the filling-in effect can be significantly stronger at the blue or UV wavelengths where the total umbral irradiance is lower and consequentially the forward-scattering proportion is larger. For a penumbral spectrum like Penumbra A, the Raman scattering transfers less than  $10^{-6}$  of the continuum photons, which is a negligible amount.

From the above estimates, we conclude that the Ring effect can be important in the umbra especially for the spectra taken close to the umbral center, and the line shape of the strong Fraunhofer line is affected by both the Ring effect and CLV effect. However, the line shape in the penumbral spectrum is dominated by the CLV effect, and the Ring effect can be safely ignored.

#### 4.2. Telluric Sodium absorption

The sodium layer existing in the Earth’s upper mesosphere originates from meteoroids (Plane 2003). Since the sodium  $D_2 - D_1$  doublet are resonance lines, their absorption features should be imprinted on the transmission spectrum if there is a significant sodium layer in the observed atmosphere. Using an average Na concentration profile measured by Fussen et al. (2004) and the cross-section data in Fussen et al. (2010), we are able to model the Na absorption for the integrated Earth atmosphere. The Na transmission spectrum for each tangential path with a minimum atmospheric altitude is calculated, and then the spectra with the minimum altitudes from 0 km to 120 km are integrated to obtain the integrated absorption spectrum. This modelled absorption spectrum is convolved to the instrumental resolution for ES-PaDONs/CFHT and the equivalent width of the  $D_1$  line is calculated to be  $0.007 \text{ \AA}$  with a maximum absorption depth of 0.08.

As stated before, the penumbral spectrum is predominantly the direct sunlight with a small component of light transmitted from the Earth atmosphere. The actual ratio between the direct sunlight and transmitted sunlight depends on the portion of the solar disk that is not occulted by the Earth. Fig. 10 shows an example of the theoretical Na absorption feature in a penumbral spectrum when 1/6 of the solar disk can be seen (i.e. similar to the Penumbra A in Fig. 1). The CLV feature of the corresponding penumbral to bright Moon ratio spectrum is also shown for comparison.

We emphasise that the CLV features shown here are from observations, not a theoretical model. It is difficult to theoretically model the precise line profile for a given penumbral spectrum

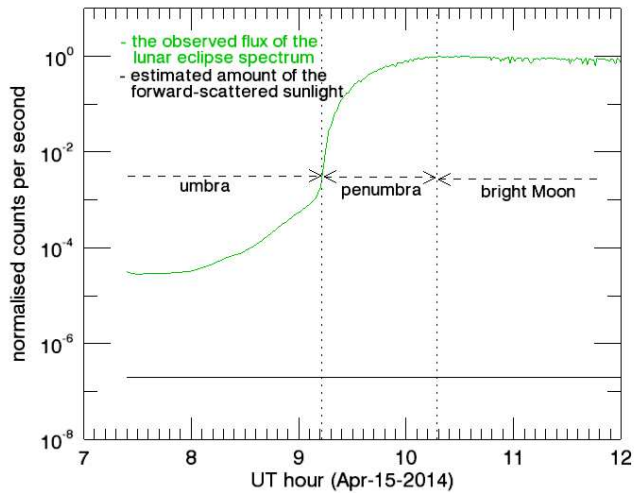


**Fig. 9.** Flux of the lunar eclipse spectrum and the forward-scattered sunlight. The green line is the total observed counts per second between 550–650 nm of the 292 lunar spectra that were observed with CFHT during the 2014-Apr-15 lunar eclipse. The numbers are normalised to a bright Moon spectrum taken at the meridian. The plot can be approximately regarded as the light curve of the eclipsed Moon, which is normalised to the flux of the unobstructed Sun (i. e. the flux for the bright Moon). The black solid line is the estimated forward-scattered sunlight from García Muñoz & Pallé (2011) and the amount used here is  $2 \times 10^{-7}$  of the flux from the unobstructed Sun.

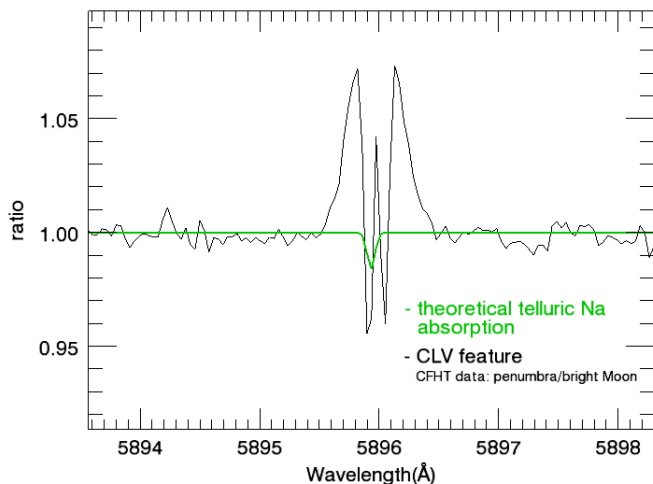


**Fig. 10.** Theoretical telluric Na absorption and the CLV feature for the Na I D<sub>1</sub> line (5896 Å). A RV correction has been applied to the CFHT spectra. The CLV feature still dominates the line profile in a penumbral spectrum, which makes the telluric Na absorption difficult to detect.

because the line profile changes quickly with time as the eclipse proceeds (as demonstrated in Fig. 3 with H $\alpha$ ). Also the Rossiter-McLaughlin effect and the convective blueshift contribute to the change of the line profile and the line position. Thus, although the telluric sodium doublet should theoretically be present in the penumbral spectrum, its relatively weak absorption features are masked by the significant line profile change of the solar sodium doublet.

### 4.3. The CLV effect in exoplanet transits

The standard way of detecting atomic or molecular species in an exoplanet atmosphere is by observing the corresponding absorption lines in and out of transit. Charbonneau et al. (2002) detected Na I for the first time in an exoplanet atmosphere using the transit spectro-photometric method. They observed the spectra of the Na I D lines in HD 209458 while the planet was transiting the star and compared this with data out of transit. The absorption depth of Na I D lines in transit was seen to be deeper than that out of transit, which indicates the existence of neutral sodium somewhere in the planetary atmosphere. Since the planet blocks different parts of the stellar disk during the transit, the CLV effect of the stellar lines needs to be considered when comparing the line depths. Charbonneau et al. (2002) modelled the effect of the CLV of the Na I D lines and found the difference of the absorption depth between in-transit and out-of-transit caused by the CLV effect to be  $1.5 \times 10^{-5}$  for a bandwidth of 12 Å (5887–5899 Å). This value is at the level of photon-noise and its effect on the Na I detection in the atmosphere of HD 209458b is negligible given that the actual observed difference of the Na I D lines depth is  $-23.2 \times 10^{-5}$ . Thus it is safe to ignore the CLV effect for the Na I detection with a broad bandwidth like 12 Å used in Charbonneau et al. (2002). However, as can be seen from Fig. 6, the Na I D line CLV feature is prominent in a high-resolution spectrum and a 12 Å bandwidth will smear the CLV feature. If the observation is performed at a higher resolution that can resolve the line profile well, and a narrower bandwidth is used, the Na I D CLV feature would become more prominent.

As can be seen from the solar limb to centre ratio spectrum in Fig. 4b, the Na I D CLV feature is relatively weak and becomes more significant for other strong Fraunhofer lines such as H $\alpha$  and Ca II H&K. Observations at blue and UV wavelengths should deal more carefully with the CLV since the effect becomes more prominent at shorter wavelengths.

Late-type dwarf stars are thought to be promising targets for exoplanet atmosphere detection because the planetary transit depth is larger due to the relatively large planet-star radius ratio. However, the CLV of the strong molecular absorption lines in these stars could affect the corresponding molecular detections in exoplanet atmospheres. Fig. 11 shows the CO band CLV feature in an M-type dwarf calculated from a Kurucz grid model<sup>2</sup>. From the model, we find that the CO band is deeper in the limb spectrum than in the centre spectrum. This indicates that when a planet transits the centre part of an M-type dwarf, the CO band in the observed spectrum will be deeper compared to the spectrum out of transit, which could potentially be interpreted as a planetary CO absorption feature.

We are currently performing a more detailed quantitative analysis of the CLV effect during exoplanet transits. Here we mention three general aspects that affect the strength of the CLV feature. The first concerns the star itself. The CLV effect depends on the physical parameters and the chemical abundances of the star so that different stellar types and different spectral lines will exhibit different CLV signatures. The second aspect is the geometry of the planet transit system, including both the planet-to-star radius ratio, which determines the obscured proportion of the stellar disk and the impact parameter of the planet's transit trajectory on the stellar disk. The planet will transit only the limb part of the stellar disk if  $b$  is close to 1 ( $b$  is the impact parameter in the unit of the stellar radius), while both the limb and the centre of the stellar disk will be blocked

<sup>2</sup> <http://kurucz.harvard.edu/grids.html>



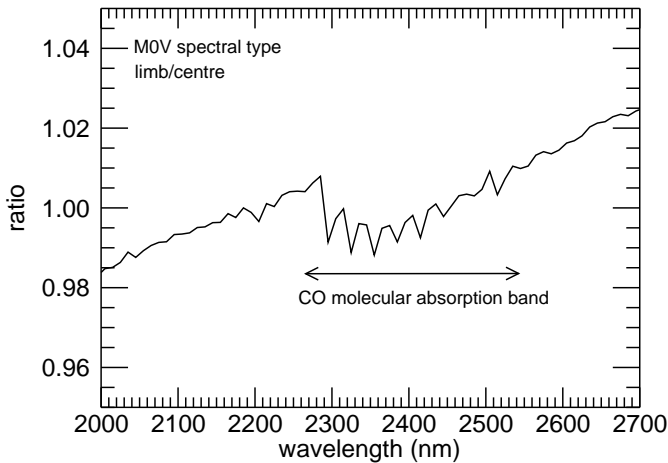


**Fig. 11.** The CLV features of a M0V type star around the CO band. The spectrum shown is the flux ratio of the limb spectrum ( $\mu = 0.2$ ) to the centre spectrum from the Kurucz stellar model. The ratio is normalised to 1 at 2200 nm. The CO absorption band shows a different limb darkening compared to the adjacent continuum.

if  $b = 0$  (i.e. edge-on). As can be seen from the lunar eclipse data in Fig. 3, the actual CLV feature varies with the phase of the transit. The third aspect is related to the observational method. For example, the spectral resolution and the chosen bandwidth for the analysis will determine the apparent strength of the CLV effect.

Consequently the theoretical CLV modelling work for different stellar types needs to be well-chosen for the precise characterisation of exoplanet atmospheres. An additional application of these studies is the employment of the CLV effects during the exoplanet transit to serve as a probe for the study of the star itself (Dravins et al. 2014).

## 5. Conclusions

Using a sequence of lunar eclipse spectra observed with the CFHT, we have demonstrated the significant center-to-limb variations of the solar Fraunhofer lines. Generally, the Fraunhofer lines are deeper in the centre spectrum than in the limb spectrum and the CLV features are stronger towards the blue and UV wavelength range. The CLV of the Na I D lines is weaker compared to other strong lines.

This CLV effect is especially important for studying the atom or ion absorptions in the transmission spectrum of the Earth's atmosphere. For previous lunar eclipse observations, the Ca II absorption feature in Pallé et al. (2009) and the Na I D lines feature in Vidal-Madjar et al. (2010) and Arnold et al. (2014) are shown to be most likely due predominately to the CLV of the corresponding solar lines instead of the Na I or Ca II absorption in the Earth's atmosphere. Although there are variable Ca II and Na I layers in the Earth's atmosphere, the reliable detection of their relatively weak absorption features is difficult because of the CLV features.

The CLV effect needs to be considered in searches for atom or ion absorptions in exoplanet atmospheres using the transit technique, especially when observing at high spectral resolution or at blue or UV wavelengths where the CLV is prominent. Molecular absorptions in M-type stars also exhibit CLV features, thus future molecular detections in planets transiting M-type stars should employ an accurate stellar model.

**Acknowledgements.** This research uses data obtained through the Telescope Access Program (TAP), which is funded by the National Astronomical Observatories, Chinese Academy of Sciences, and the Special Fund for Astronomy from the Ministry of Finance. The study is supported by the National Natural Science Foundation of China under grants Nos. 11390371 and 11233004. We thank the CFHT team for the observations. The authors thank the referee for useful suggestions. Fei Yan acknowledges the support from ESO-NAOC studentship.

## References

- Allende Prieto, C., Asplund, M., & Fabiani Bendicho, P. 2004, *A&A*, 423, 1109  
 Arnold, L., Ehrenreich, D., Vidal-Madjar, A., et al. 2014, *A&A*, 564, A58  
 Athay, R. G. 1972, *Radiation Transport in Spectral Lines*  
 Athay, R. G., Lites, B. W., White, O. R., & Brault, J. W. 1972, *Sol. Phys.*, 24, 18  
 Brault, J. & Testerman, L. 1972, *Kitt Peak solar atlas*  
 Brogi, M., Snellen, I. A. G., de Kok, R. J., et al. 2012, *Nature*, 486, 502  
 Charbonneau, D., Brown, T. M., Noyes, R. W., & Gilliland, R. L. 2002, *ApJ*, 568, 377  
 Colón, K. D., Ford, E. B., Redfield, S., et al. 2012, *MNRAS*, 419, 2233  
 Dravins, D., Ludwig, H.-G., Dahlén, E., & Pazira, H. 2014, *ArXiv e-prints*  
 Fossati, L., Bagnulo, S., Elmasli, A., et al. 2010, *ApJ*, 720, 872  
 Fussen, D., Vanhellemont, F., Bingen, C., et al. 2004, *Geophys. Res. Lett.*, 31, 24110  
 Fussen, D., Vanhellemont, F., Tétard, C., et al. 2010, *Atmospheric Chemistry & Physics*, 10, 9225  
 García Muñoz, A. & Pallé, E. 2011, *J. Quant. Spec. Radiat. Transf.*, 112, 1609  
 García Muñoz, A., Zapatero Osorio, M. R., Barrena, R., et al. 2012, *ApJ*, 755, 103  
 Grainger, J. F. & Ring, J. 1962, *Nature*, 193, 762  
 Grillmair, C. J., Burrows, A., Charbonneau, D., et al. 2008, *Nature*, 456, 767  
 Hedelt, P., von Paris, P., Godolt, M., et al. 2013, *A&A*, 553, A9  
 Koesterke, L., Allende Prieto, C., & Lambert, D. L. 2008, *ApJ*, 680, 764  
 Kurucz, R. L. 2005, *Memorie della Societa Astronomica Italiana Supplementi*, 8, 189  
 Langford, A. O., Schofield, R., Daniel, J. S., et al. 2007, *Atmospheric Chemistry & Physics*, 7, 575  
 Link, F. 1972, *Advances in Astronomy and Astrophysics*, 9, 67  
 Noxon, J. F., Whipple, Jr., E. C., & Hyde, R. S. 1979, *J. Geophys. Res.*, 84, 5047  
 Pallé, E., Zapatero Osorio, M. R., Barrena, R., Montañés-Rodríguez, P., & Martín, E. L. 2009, *Nature*, 459, 814  
 Plane, J. M. 2003, *Chemical reviews*, 103, 4963  
 Quintana, E. V., Barclay, T., Raymond, S. N., et al. 2014, *Science*, 344, 277  
 Redfield, S., Endl, M., Cochran, W. D., & Koesterke, L. 2008, *ApJ*, 673, L87  
 Sing, D. K., Désert, J.-M., Fortney, J. J., et al. 2011, *A&A*, 527, A73  
 Snellen, I. A. G., Albrecht, S., de Mooij, E. J. W., & Le Poole, R. S. 2008, *A&A*, 487, 357  
 Swain, M. R., Tinetti, G., Vasisht, G., et al. 2009, *ApJ*, 704, 1616  
 Swain, M. R., Vasisht, G., & Tinetti, G. 2008, *Nature*, 452, 329  
 Vidal-Madjar, A., Arnold, L., Ehrenreich, D., et al. 2010, *A&A*, 523, A57  
 Vollmer, M. & Gedzelman, S. D. 2008, *Appl. Opt.*, 47, H52  
 Wood, P. L., Maxted, P. F. L., Smalley, B., & Iro, N. 2011, *MNRAS*, 412, 2376  
 Yan, F., Fosbury, R. A. E., Petr-Gotzens, M. G., et al. 2014, *International Journal of Astrobiology*, FirstView, 1